공학석사 학위논문

# Atomic Structure Analysis of Octahedral Rotations in Strained $SrRuO_3$ Thin Films

## $SrRuO_3$ 박막 내 팔면체 뒤틀림 현상의 원자 수준에서의 결정 구조 분석

2016년 2월


서 울 대 학 교 대 학 원

재 료 공 학 부

김 은 주

## Abstract

# Atomic Structure Analysis of Octahedral Rotations in Strained $SrRuO_3$ Thin Films

Eunju Kim

Department of Materials Science and Engineering

College of Engineering

Seoul National University

Physical properties of perovskite oxides are strongly dependent on subtle structural deformation because of the large lattice-electron correlations, therefore, it is essential to obtain accurate structural information to understand the underlying mechanism of structure-property relationship. Particularly, perovskite oxide thin films which are subject to the substrate-induced stress present a range of intriguing physical properties. In this study, we investigated strain effects on $SrRuO_3$ thin films by measuring $RuO_6$ octahedral rotation across the interface using high resolution scanning transmission electron microscopy-annular bright field (STEM-ABF) imaging together with electron diffraction patterns, and the corresponding changes in electronic properties.

We compared the crystal structures of $SrRuO_3$ thin films on two substrates, $GdScO_3$ (GSO) and $SrTiO_3$ (STO), which are chosen for inducing tensile/ compressive strain and having the orthorhombic and cubic structure respectively. HRTEM images and their fast Fourier transformed micrographs revealed that the SRO films consisted of different domains, with sustained and released octahedral rotation. High resolution STEM-ABF images of released octahedral rotation region demonstrate less-distorted octahedral rotation patterns both on GSO and STO substrates. Only difference was the interface region. On the GSO substrate, including the topmost layer of GSO, SRO has somewhat sustained octahedral rotation up to two unit cells, while on STO, there was almost no rotation throughout the whole film. These different results around the interface area can be ascribed to the symmetry mismatch effect. Since in both cases, SRO films have mixed structure with no big distinction, electrical property shows similar data. This study demonstrates that the octahedral rotations can be understood as the interplay between lattice mismatch and symmetry mismatch.

**Keywords:** Strain effect, octahedral rotation, lattice mismatch, symmetry mismatch, STEM-ABF imaging and $SrRuO_3$ thin film
**Student Number:** 2014-21478

# Contents

# List of Tables

# List of Figures

# Chapter 1. Introduction

Perovskite oxides which have $ABO_3$ structures have been extensively investigated over the past decades since they have a wide range of interesting physical properties such as colossal magnetoresistance, superconductivity, and charge ordering.[1] In addition, they are useful for constructing complex structures as building blocks and have potential applications in low-power electronics, energy storage, and conversion.[2] For these reasons, they have been considered as important system for studying fundamental physics as well as developing electronic devices.

Most perovskite oxides with non-cubic structures have various structural distortions on $BO_6$ octahedra and they can be categorized by three different origins - Jahn-Teller distortion (e.g. $LaMnO_3$), cation displacement (e.g. $BaTiO_3$), and octahedral rotation (e.g. $CaTiO_3$, $SrRuO_3$, $LaAlO_3$ etc.), [3] which will be discussed in further detail in the following Chapter 2.4. Among these, octahedral rotation is more often observed than others in orthorhombic perovskite oxides by rotating the rigid $BO_6$ octahedra as found in $CaTiO_3$, $SrRuO_3$, $LaAlO_3$, etc.[4,5]

Rotations of corner-sharing $BO_6$ octahedra can change B-O-B bond

---

[1] M.B. Salamon and M. Jaime, Rev. Mod. Phy. 73, 583(2001)

[2] L.W. Martin, et. al., Mater. Sci. Eng., R 68, 89 (2010)

[3] W. Lu et. al., Phys Rev B, 88, 214115 (2013)

[4] K.J.Choi et. al., Adv. Mater. 22, 759-762 (2010)

[5] W. Lu et. al., J. Appl. Phys., 113, 063901 (2013)

angles, consequently affect electronic structures such as band width. A number of related experimental results have been reported. For example, subtle changes of octahedral rotations induce phase stabilization [6], ferroelectricity[7] and magnetic ordering in some systems[8]. As the magnitude and sense of rotations play a crucial role in determining perovskite oxides' physical properties, it is essential to understand the fundamental of octahedral rotation pattern in perovskite oxides in order to design new functional materials.

In heterostructures, unexpected physical phenomena have been observed at the interface as a result of additional structural deformation while sustaining coherency between two materials with different lattice constants. In other words, strain driven by lattice mismatch have an influence on structural deformation and by extension physical properties. Therefore, there have been numerous studies on systematic choice of substrates for controlling lattice mismatch, and they mostly conducted X-ray diffraction analysis by obtaining lattice parameters. Quantitative experimental evidences, however, are still lacking because precise detection of oxygen atomic position is extremely difficult. Recent advance of annular bright field (ABF) scanning transmission electron microscopy (STEM) combined with high angle annular dark field (HAADF) imaging can be a novel method for visualizing light atoms (O, N,

[6] Y.-M. Kim et. al., Adv. Mater. 25, 2497 (2013)

[7] E. Bousquet et al., Nature, 452, 732 (2008)

[8] V. Gopalan et al., Nat. Mater, 10, 376 (2011)

Li, etc.)[9].

To examine the strain effect on octahedral rotations, we focus on $SrRuO_3$ (SRO), which is a popular topic among materials scientists and physicists. Due to its intermediate electron correlation and large magneto crystalline anisotropy, it has been regarded as an appropriate system for studying magnetism and structure-property relationships.

In this paper, the octahedral behaviors to different signs of strains in epitaxial $SrRuO_3$ films were investigated. Two different substrates, (001) $SrTiO_3$ (STO) and (110) $GdScO_3$ (GSO), were used for deposition as they have acceptable lattice mismatches with $SrRuO_3$ and can impose the opposite sign of strain. STO substrates apply compressive strain of -0.523% along [100] in-plane direction and GSO substrates induce tensile strain of +1.18% along [110], +0.99% along [001] in-plane direction on SRO thin films. We also varied the thickness of films, 8nm and 24nm, in order to observe the effect of strain relaxation throughout the whole film. Furthermore, crystal symmetry was important factor as well. GSO substrate has orthorhombic and STO has cubic structure so that we could compare the effect of substrate symmetry at the same time.

We found out that under tensile strain, SRO films have two different domains which have octahedral rotations and/or not. It was confirmed by FFT diffraction patterns. From high resolution STEM-ABF image, it has less-

[9] R. Aso et al., Sci. Rep. 3, 2214 (2013).

distorted octahedra pattern as a result of fully stretched Ru-O-Ru bonds, sustaining the network of corner-sharing octahdera. However, near the interface region sustained subtle octahedral rotation due to symmetry mismatch of GSO substrate, orthorhombic. On STO substrates, SRO films were deposited with c-axis along in-plane and they are also consist of two different domains. ABF images show much released octahedral rotation not only the upper area but also the interface region as a result of symmetry effect.

For further investigation, we measured the Curie temperature (Tc) of all films to explore structure-property relationship. All samples show similar Tc, which is consistent with structural results. Our study demonstrated that there are close links between structure and physical property and the octahedral rotations play a key role for determining electronic structure.

# Chapter 2. Literature Survey

## 2.1 Materials of Interest – $SrRuO_3$

The main material of this study, $SrRuO_3$ (SRO) is one of functional oxide materials exhibiting a number of intriguing physical properties. [10] It shows high thermal conductivity, strong chemical stability, and outstanding resistance to corrosion, whose properties are appropriate for device applications. These good functionalities lead that SRO thin films have been widely used as electrodes or thin barriers for various oxide devices. [11]

It is reported that SRO has a $GdFeO_3$ type orthorhombic structure (space group of Pbnm, No.62) at room temperature with lattice parameters a=5.57 Å, b=5.53 Å and c=7.85 Å.[12] It can also be described in terms of pseudo-cubic lattice parameters, $a_{pc}=b_{pc}=\sqrt{(a^2+b^2)}/2$ and $c_{pc}=c/2$. (The subscript "pc" stands for pseudo-cubic.) as depicted in **Fig 1**. In Glazer's notation, the rotation of $RuO_6$ is described by (a-a-c+).[13] It means that $RuO_6$ octahedra rotate out-of-phase about [100]pc, [010]pc directions and in-phase about [001]pc. SRO is paramagnetic and conductive at room temperature and ferromagnetic below the Curie temperature of ~150K.

As aforementioned, due to its moderate correlation, SRO is appropriate for studying structure-property relationship. Therefore, structural phase transition has been extensively investigated. For example, it is reported

[10] G. Koster *et al.*, Rev. Mod. Phys. 84, 253 (2012).
[11] L. Antognazza *et al.*, Appl. Phys. Lett. 63, 1005 (1993).
[12] C. W. Jones et al., Acta. Crystallogr, 45, 365 (1989)
[13] M. W. Lufaso et. al., Acta. Crystallogr, Sect. B:Struct. Sci. 60, 10 (2004)

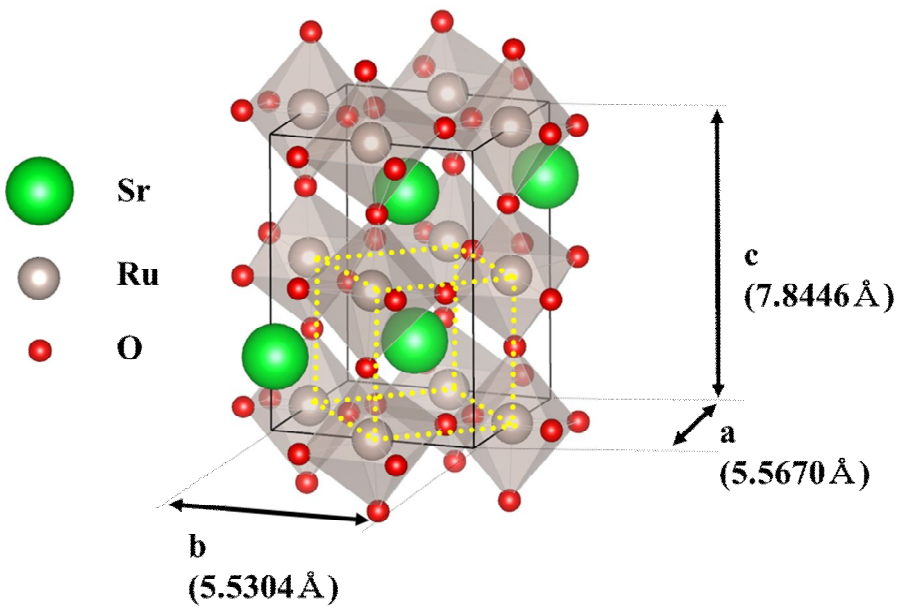


**Figure 1 Schematic view of orthorhombic $SrRuO_3$ unit cell. A cubic inside with yellow dashed line exhibits the pseudo-cubic SRO unit cell structure.**

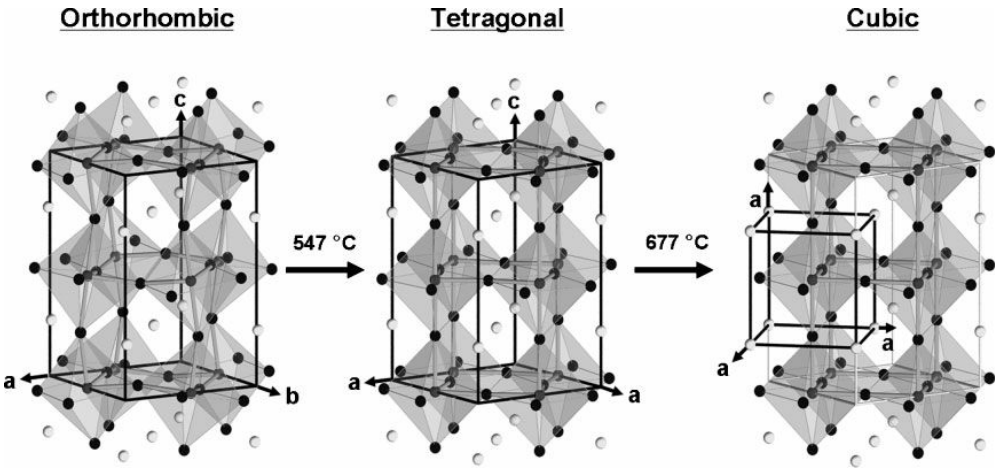


**Figure 2 A schematic representation of phase transition as temperature increases in unstrained bulk $SrRuO_3$ [14]**

that bulk $SrRuO_3$ undergoes a series of phase transformation from orthorhombic to higher-symmetry perovskite with increasing temperature.[14] As temperature goes up, the orthorhombic structure transforms into tetragonal (space group I4/mcm) around 550℃ and cubic (space group Pm3m) around 680℃. In tetragonal perovskite structure, $RuO_6$ octahedra only rotates around [001] and there are no rotations in cubic perovskite as shown in **Fig 2**.

We can simply obtain the electronic structure of SRO from atomic orbitals. Due to the octahedral crystal environment, the fivefold degeneracy of Ru 4*d* orbitals are divided into two groups, raising $4d(e_g)$ levels above $4d(t_{2g})$ levels as illustrated in **Fig 3**. Four electrons fill the three $4d(t_{2g})$ levels by Hund's rules, resulting in spin state S=1.[15] According to Allen[16] and Singh[17] who calculated first-principle band structure, SRO is itinerant ferromagnetic with ground-state moment of 1.5-1.6 $\mu_B$. Furthermore, Singh found out that this ground-state moment is only valid for the actual orthorhombic structure and for the ideal cubic it is 1.17 $\mu_B$. This result was confirmed again by comparing with $CaRuO_3$, which has twice larger octahedral tilt angle than $SrRuO_3$. Large tilt angle leads to mixing bands with $e_g$ and $t_{2g}$, which in turn reduces both the Stoner factor and the total band width. To sum, the electronic structure of perovskite, especially SRO, is so sensitive to structural modification.

---

[14] K. J. Choi el al., Adv. Mater. 22, 759 (2010)
[15] Cox et al., J. Phys. C 16, 6221 (1983)
[16] Allen et. al., Phys. Rev. B 53, 4393 (1996)
[17] Singh el. Al., J. Appl. Phys. 79, 4818 (1996)

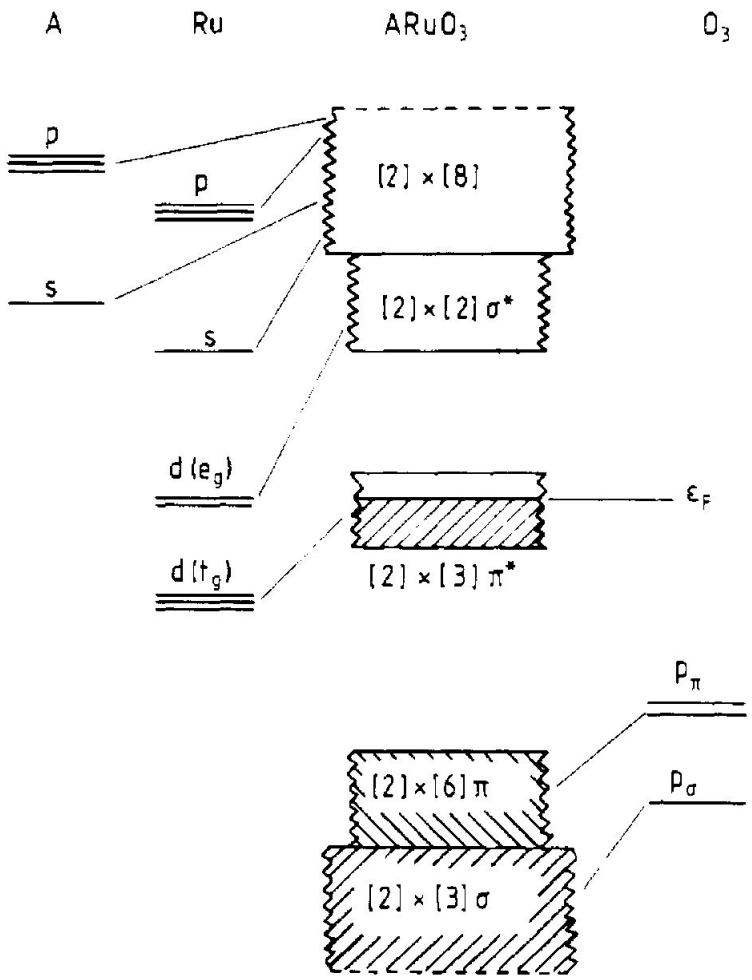


**Figure 3 Schematic low-spin one-electron energy level diagram for a perovskite ruthenate $ARuO_3$[15]**

## 2.2 The experimental studies on $SrRuO_3$ thin films

It is well known that compared to bulk form of materials, thin film form has advantages as a model system for studying because it is easier to control the crystal structure by manipulating extrinsic variables such as pressure, thickness and the choice of substrates. Since thin films of $SrRuO_3$ is also considered as the most important form of this material for both theoretical study and device applications, epitaxial SRO films have been successfully grown on various substrates by different methods including 90° off-axis sputtering, molecular beam epitaxy, reactive thermal evaporation, metal organic chemical vapor deposition, and pulsed laser deposition.[18] Depending on these growth methods and deposition conditions, the quality of SRO films is determined.

In addition, the surface of substrate should be well-defined not to form defects. Not only cleaning the surface with organic solvents but also proper chemical treatment and annealing should be followed to form single-termination layer because the terminating layer has a great influence on the initial growth process. The most commonly used substrate is $SrTiO_3$ and the methods for making $TiO_2$ single-termination was developed by Kawasaki.[19]

[18] G. Koster et. al., Rev. of Mod. Phys. 84, 253 (2012)
[19] Kawasaki et. al., Science 266, 1540 (1994)

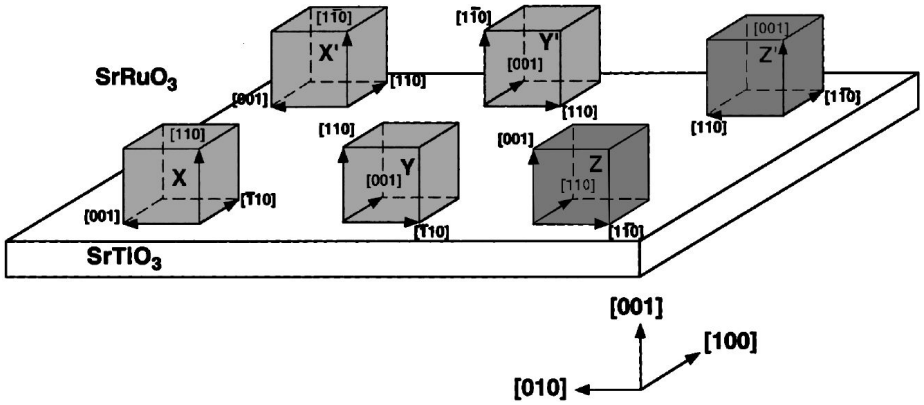


**Figure 4 A schematic figure of six possible orientations of SRO on STO substrates with pseudo-cubic unit cell [20]**

Especially, on STO substrate, SRO can be grown having multiple domain structures. As shown in **Fig 4**, there are six different possible orientations for SRO on STO: with its (110) plane parallel to the STO (001) surface, or (001) plane parallel to the STO (001) etc.[20] Depending on the growth method or condition, these domains can coexist, and indeed, many studies have been reported about multi-domain SRO thin films mainly using XRD and TEM. However, in general, the optimum physical properties take place in single crystalline materials with single-domain structure, so that the condition for single domain structure has been widely investigated as well. To date, it is accepted that high miscut substrate (>2° ) is required for making single domain SRO.[21]

[20] J. C. Jiang *et. al.,* Appl. Phys. Lett., 72, 23 (1998)
[21] G.herranz et. al., Phys. Rev. B 71, 174411 (2005)

## 2.3 The importance of structural transition in $SrRuO_3$

As mentioned, bulk SRO undergoes phase transition from orthorhombic to higher-symmetry perovskite such as tetragonal and cubic structure with increasing temperature. For thin films of SRO, the same transition happened but lower transition temperatures were observed.[22] This results can be ascribed to the strain effect. Like this, epitaxial thin films are susceptible to substrate-induced strain. Therefore, in order for SRO to be grown coherently as single crystalline, the choice of appropriate substrate is crucial because close lattice matching is strongly required.

In **Table 1**, we summarized the list of studies focusing on the structural deformation by substrate-induced strain in SRO system within 10 years. It is seen that there is no clear conclusion but a lot of controversial results have been reported. For example, under tensile strain, SRO is supposed to have monoclinic, tetragonal or orthorhombic. In part, this is because of the difference in growth technique and condition. However, the analysis method can be another factor. In other words, these studies were mostly conducted using XRD analysis and XRD has intrinsic limitation to study thin film microstructure. At first, XRD signal is obtained from the entire specimen so we cannot get microscopic information. And when the films are too thin, so the intensity of signal may not enough to be analyzed. On the other hand, TEM can be a powerful tool for microscopic structure analysis. On top of the

[22] Maria J. P. et al., Appl. Phys. Lett. 76, 3382 (2000)

conventional TEM, Cs-corrected TEM was recently developed, so nowadays high resolution STEM imaging at sub-angstrom scale is possible. In particular, ABF imaging is suitable for detecting light elements such as oxygen, it can be helpful to investigate $BO_6$ octahedral rotation pattern.

**Table 1 Summary of studies on substrate-induced strain effect in structural deformation of SRO thin films**

| | Compressive strain | Tensile strain | Analysis method |
|---|---|---|---|
| A.T.Zayak (2006) | Monoclinic | Monoclinic | DFT calculation |
| A.Vailionis (2011) | NGO substrate<br>Monoclinic(a+a-c0) | DSO substrate<br>Tetragonal(a+a-c0) | XRD |
| S.H.Jang (2011) | STO substrate<br>< 70nm : tetragonal<br>> 70nm : orthorhombic | | XRD |
| Daisuke Kan (2013) | | GSO substrate<br><16nm : monoclinic<br>>16nm : tetragonal | XRD, TEM study |
| W.Lu (2015) | NGO substrate<br>Tetragonal(a0a0c-) | KTO substrate<br>Orthorhombic(a-a-c+) | XRD, TEM study |

## 2.4 Octahedral rotations in $ABO_3$ perovskite materials

The ideal structure of perovskite oxides with $ABO_3$ is basically simple cubic where A cations occupy the corner sites and B-O-B bond angle is 180° resulting in corner-connected $BO_6$ octahedra. Indeed, only few oxides exhibit this ideal cubic and most materials adopt distorted structures with lower symmetry. Whether the perovskite material has the cubic or not can be approximately predicted according to Goldschmidt's tolerance factor t. It is the ratio or ionic radius of A, B and oxygen as shown below.

$$t = \frac{\left(r_A + r_O\right)}{\sqrt{2}\left(r_B + r_O\right)}$$

The distorted perovskite oxides with lower symmetry than cubic is associated with three different origins which are Jahn-Teller distortion, cation displacement, and rotation/tilting of rigid octahedra. Through these, shape, size and connectivity of octahedra are sensitively varying.

Among them, octahedral rotation is the most commonly occurring distortion. Therefore, to systematically classify the existing octahedral tilting pattern, Glazer's notation has been developed and widely accepted. The tilt system is conveniently written using three letters a, b, c and superscripts +, - and 0. Three letters denote each pseudo-cubic axis and the sense of the rotations are described by the superscripts +, −, or 0. These indicates whether adjacent octahedral rotate in-phase (+), out-of-phase (-) or not at all (0). According to this notation, up to 23 tilt patterns are possible.

Though some studies dealing with octahedral distortion of perovskite tend to use two terms, 'octahedral tilting' and 'octahedral rotation' without distinction, there are conventionally separate definitions for them. As shown in **Fig 5** and **6**, the rotation along z axis is referred as 'rotation', and it is defined as $(90^\circ - \Omega)/2$ where $\Omega$ is the angle among three oxygen ions. On the other hand, 'tilting' angle is given by $(180^\circ - \Theta)/2$ where $\Theta$ is the bond angle of B-O-B along z-axis. [23]

[23] A.T.Zayak et. al., Phys. Rev. B., 74, 094104 (2006)

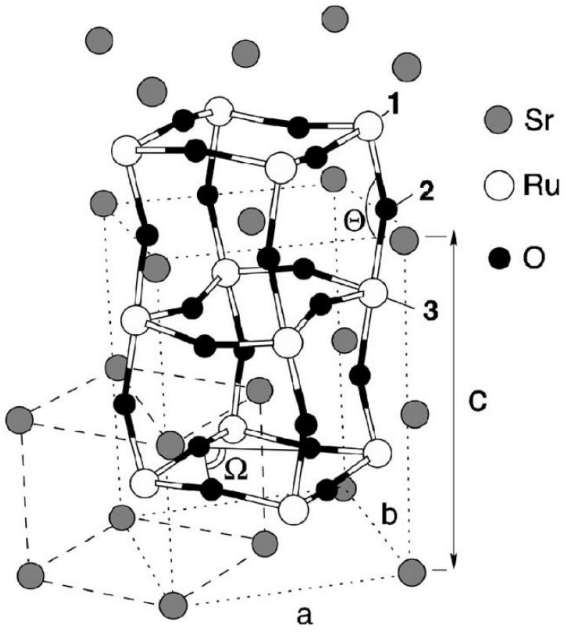


**Figure 5 The crystal structure of $SrRuO_3$ showing distortion angles Ω and Θ[23]**

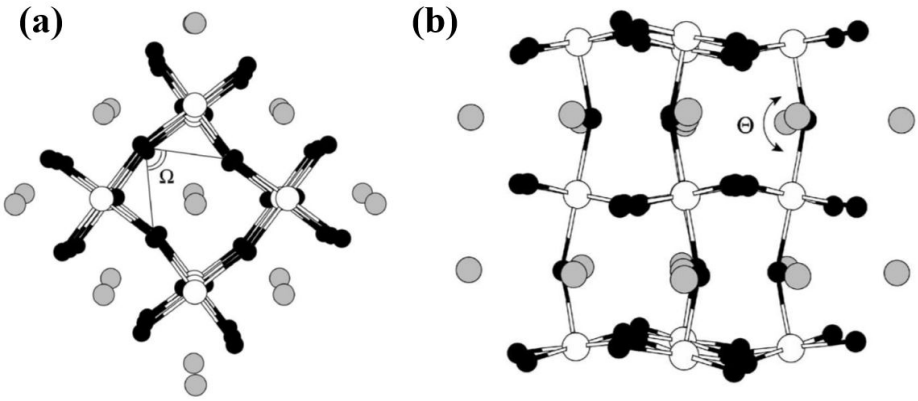


**Figure 6 (a) The top view of $SrRuO_3$ showing rotation along z-axis, (b) The tilting of SRO projected along y-axis[23]**

# Chapter 3. Experimental Details

## 3.1 Growth and characterization of $SrRuO_3$ thin films

All the $SrRuO_3$ thin films were fabricated by pulsed laser deposition technique on (110) GSO, which has an orthorhombic structure with a=5.48 Å, b=5.75 Å and c=7.93 Å and (001) STO, which has a cubic structure with a=3.905 Å. The lattice mismatches between substrates and SRO film, which were calculated by $(a_{sub}-a_{SRO})/a_{SRO}*100(\%)$, were +1.18% and -0.523%, respectively. The lattice parameters and strain along specific direction are listed in **Table 2**.

**Table 2 List of lattice parameters and strain along specific directions of bulk SrRuO3, GdScO3 and SrTiO3.**

| | Lattice parameters | | | | | Strain (%) | |
|---|---|---|---|---|---|---|---|
| Materials | a(Å) | b(Å) | c(Å) | γ(°) | $a_{pc}$(Å) | [001] | [1-10] |
| Bulk $SrRuO_3$ | 5.567 | 5.530 | 7.845 | 90 | 3.93 | - | - |
| $GdScO_3$(110) | 5.45 | 5.75 | 7.93 | 90 | 3.96 | +0.99 | +1.18 |
| $SrTiO_3$(100) | 3.905 | 3.905 | 3.905 | 90 | 3.905 | -0.59 | -0.523 |

In order to get atomically flat surfaces of substrates, GSO substrates

were annealed at 1000℃ for 6 hours and STO substrates were treated by BHF etchant for 30s and annealed at 1100℃ for 1h following the method developed by Kawasaki et al. By doing this, we could obtain single termination surfaces, in case of STO, $TiO_2$ termination.

SRO films were deposited with KrF excimer laser( $\lambda$ =248nm) with 3Hz repetition rate under 700℃ and oxygen partial pressure of 100mTorr. Two different thickness-SRO films, 8nm and 24nm, were grown using *in situ* high-pressure reflection high-energy electron diffraction (RHEED). Oscillations of RHEED spots were used to control film thickness confirming step-flow growth mode at the same time.

The surface morphology of films was investigated by atomic force microscopy (AFM). The crystalline quality and epitaxial arrangement were determined using high-resolution X-ray diffraction (HRXRD).

## 3.2 Transmission Electron Microscopy (TEM) analysis

Cross-sectional TEM specimens were fabricated along [001] and [1-10] of GSO substrates and [100] or [010] of STO substrates by focused ion beam (FIB) method.

Electron diffraction patterns and high resolution scanning TEM images were recorded in ARM equipped with a spherical aberration corrector in Seoul National University and Sungkyunkwan University operated at 200KV.

## 3.3 Physical Properties Measurement System (PPMS)

Transport properties of films were examined by physical property measurement system (PPMS; Quantum design) using 4-point probes method. Four copper wires were attached on the SRO surface using Ag epoxy and annealed for 15min at 150℃. The electrical resistance as a function of temperature ranging from 300K to 2K were measured without magnetic fields.

# Chapter 4. Results and Discussion

## 4.1 Growth and characterization of $SrRuO_3$ thin films

We recorded the intensity of RHEED(Reflection High Energy Electron Diffraction) spots during SRO deposition as shown in **Fig 7**. After few oscillations, the intensity gradually increased and then remained constant. It can be interpreted as the transition from two-dimensional layer by layer growth to step-flow growth mode. Each oscillation was sustained for about 30s indicating the time for single layer formation.

As shown in **Fig 8**, AFM images exhibit that SRO films have atomically smooth surface with small roughness (< 1nm) showing clear step-terrace structure. The step height was determined from line scan profile and found out to be about 0.4nm, unit-cell height. Line scan profile was obtained along the line drawn in the image with red line.

The XRD spectra show that SRO thin films are well stabilized with pseudo-cubic perovskite structure (see **Fig 9**). There were no other secondary phases in scanning range. We confirmed that SRO films were deposited on substrates epitaxially. Based on the Laue oscillations, we could calculate film thicknesses confirming smooth surfaces and interfaces at the same time. FWHM values of films were shown in **Fig 9** (b) which were found to be 0.03-0.06 assuring high-quality of samples.

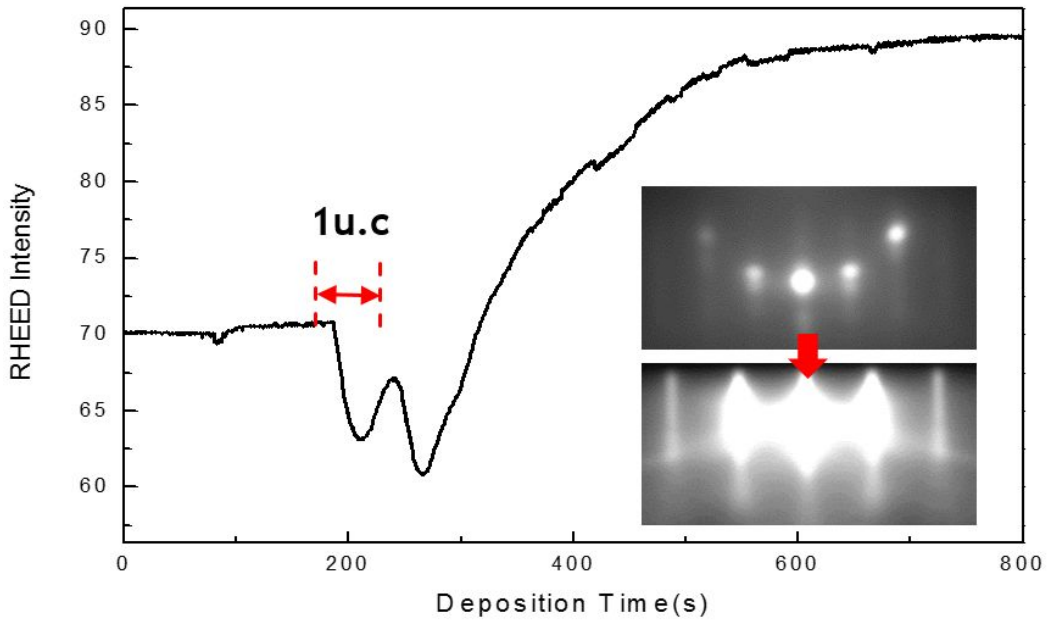


**Figure 7 Oscillation of RHEED spot**

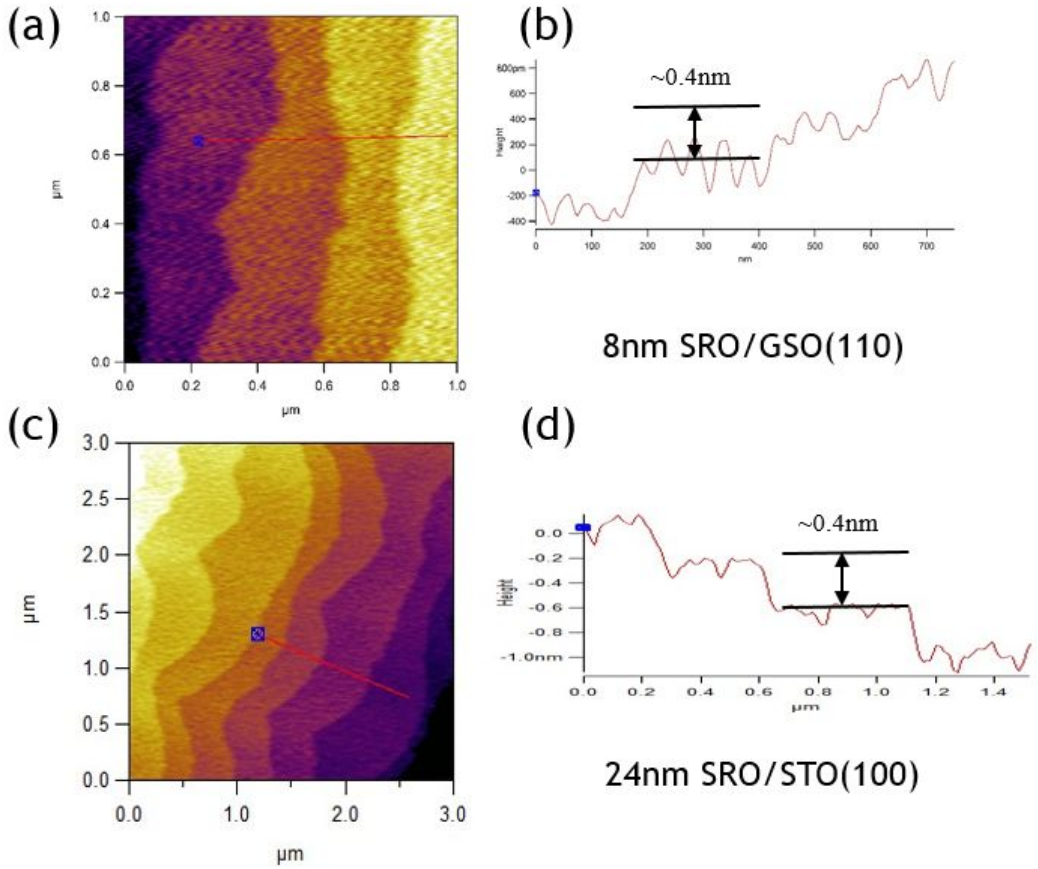


**Figure 8 AFM images of SRO thin films of (a) 8nm on GSO substrate, (b) line profile along the red line drawn in (a), (c) 24nm on STO substrate, line profile along the red line drawn in (c)**

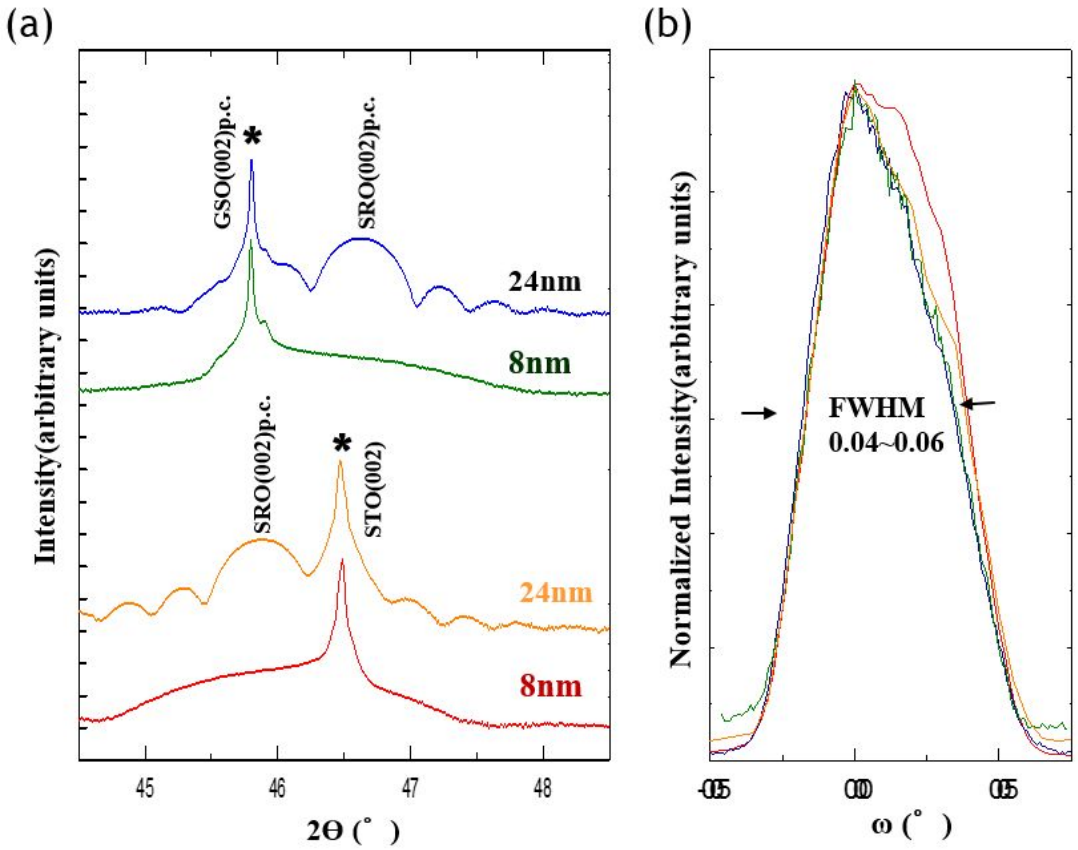


**Figure 9 XRD scan of SRO thin films (a) 2theta-omega scan (b) rocking curve**

## 4.2 Transmission Electron Microscopy (TEM) analysis

### 4.2.1 $SrTiO_3$ thin films on $GdScO_3$

**Fig 10** shows high resolution TEM images and fast Fourier - transformation (FFT) diffraction patterns of 8nm SRO films on GSO along [001] and [1-10] zone axes. As we expected, $SrRuO_3$ is grown along the [110] direction which is the same as $GdScO_3$ (110) substrate having an epitaxial relationship.(see Fig 11) From the high resolution image, it is seen that there is a sharp interface sustaining a uniform thickness without any misfit dislocation. FFT patterns from this HR image present that there are two different domains. Except for the fundamental peaks, some regions have additional peaks, which we indexed as 1/2(110). The presence of 1/2(110), half-integer reflection peak, reveals SRO films have octahedral rotation. In contrast, the absent of 1/2(110) peak is identified to be released octahedral rotation. This phenomenon happened when observed from [1-10] zone axis as well.

For thicker SRO film, 24nm, the exact same results were obtained showing SRO films consisting of two different domain. We could not find any thickness dependency between 8nm and 24nm SRO films. In order to investigate the distribution of domains, we collected HR images as many as possible and carried out statistical analysis. Consequently, about 62% of SRO films have the region without half-integer peak, in other words released rotation. The size of each domain varies from 10nm to 720nm so we conclude

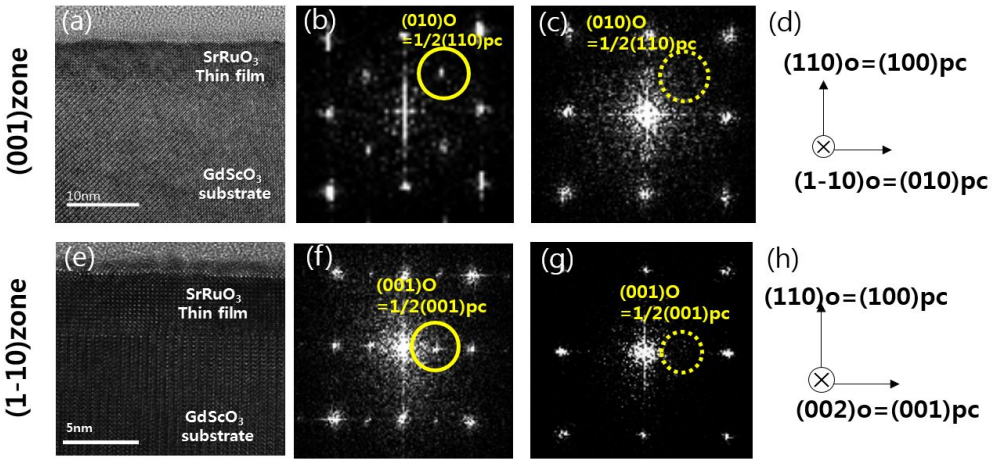


**Figure 10. HRTEM images and FFT patterns of 8nm SRO thin film on GSO substrate along [001] for (a),(b),(c) and [1-10]zone axis for (d),(e),(f). (d) and (e) show orientation relationships for each zone axis.**

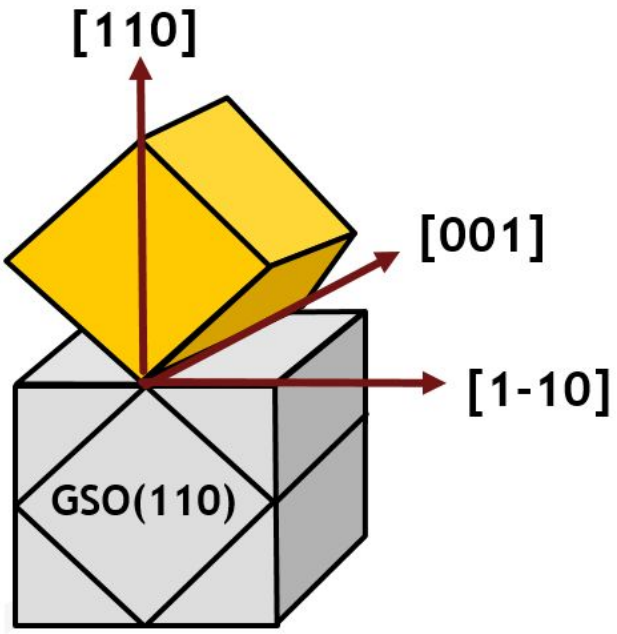


**Figure 11 Schematic image showing the epitaxial relationship between $GdScO_3$(110) substrate and $SrRuO_3$ thin film**

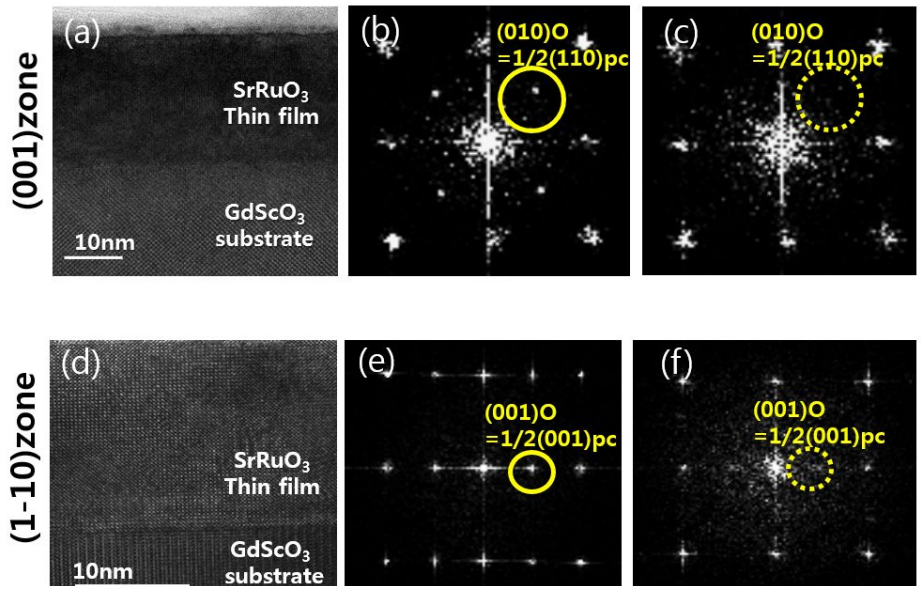


**Figure 12 HRTEM images and FFT patterns of 24nm SRO thin film on GSO substrate along [001] for (a), (b), (c) and [1-10] zone axis for (d),(e),(f).**

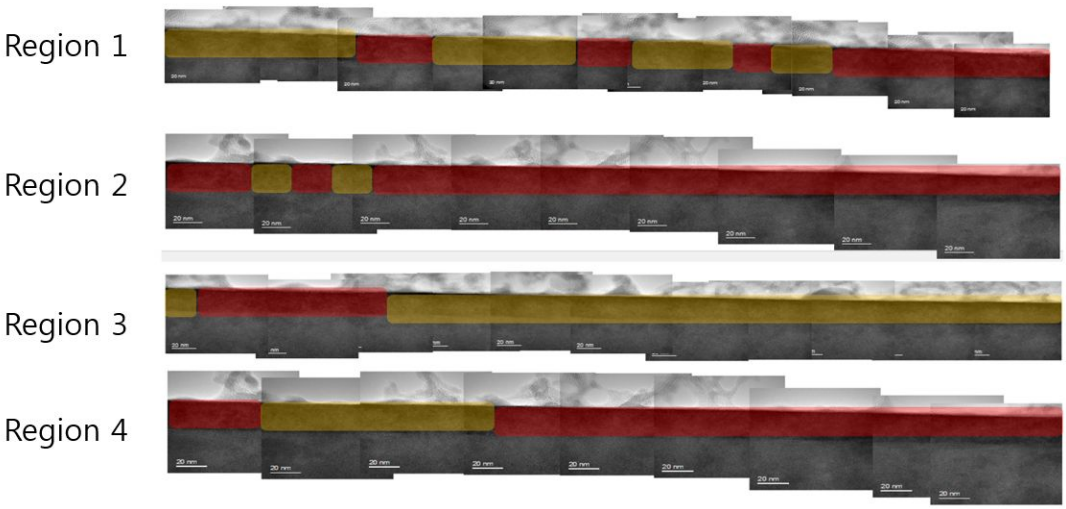


**Figure 13 Statistical analysis for investigating the distribution of two different domains. Red area shows released octahedral rotation region, while yellow area indicate sustained octahedral rotation region.**

that these two different domains are randomly distributed.

For further advanced analysis, we carried out high-resolution STEM measurement, especially using ABF technique, for detecting the exact position of oxygen atoms. **Fig 14** exhibits low magnification HAADF and ABF images of interface region. FFT diffraction patterns obtained from these images are shown in **Fig 14 (c)** and **(d)**. Unlike the GSO substrate, SRO thin films has no half- integer peak so we can expect to confirm released octahedral rotation.

Using high magnification ABF image, we conducted image filtering, contrast-inversion and maximum peak finding processes. Then we linked adjacent oxygen atoms forming diamond shape. By doing this we could locate overall octahedral pattern (See **Fig 15**). For clarity, we superimposed schematic illustration of SRO and GSO. Although it is clearly demonstrated that SRO has less rotated octahedra than GSO substrate, it is required to get quantitative data for exact comparison.

**Fig 16** shows the transition of octahedral rotation angle across the SRO/GSO interface which was obtained from ABF image (**Fig 15**). The rotation angle was determined by averaging from 15 different columns. The standard deviation is shown as error bars. The dotted lines (red and blue) are drawn to indicate the octahedral tilt angles of bulk SRO and bulk GSO. This graph reveals that in GSO substrate, octahedral rotation angle is similar with that of bulk GSO except for the top layer. At the interface region(yellow box), rotation angle gradually increases from 156° to 175° . Above two unit cell

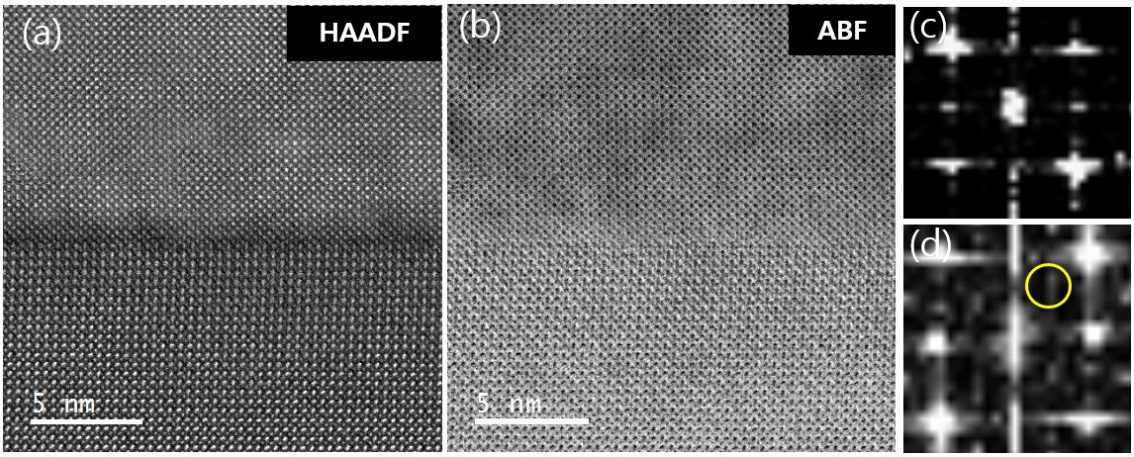


**Figure 14 Low magnification (a) HRSTEM-HAADF and (b) ABF image of interface area in 24nm SRO on GSO substrate, FFT pattern of (c) SRO thin film and (d) GSO substrate. Yellow circle in (d) indicates the existence of half integer peak, 1/2(110).**

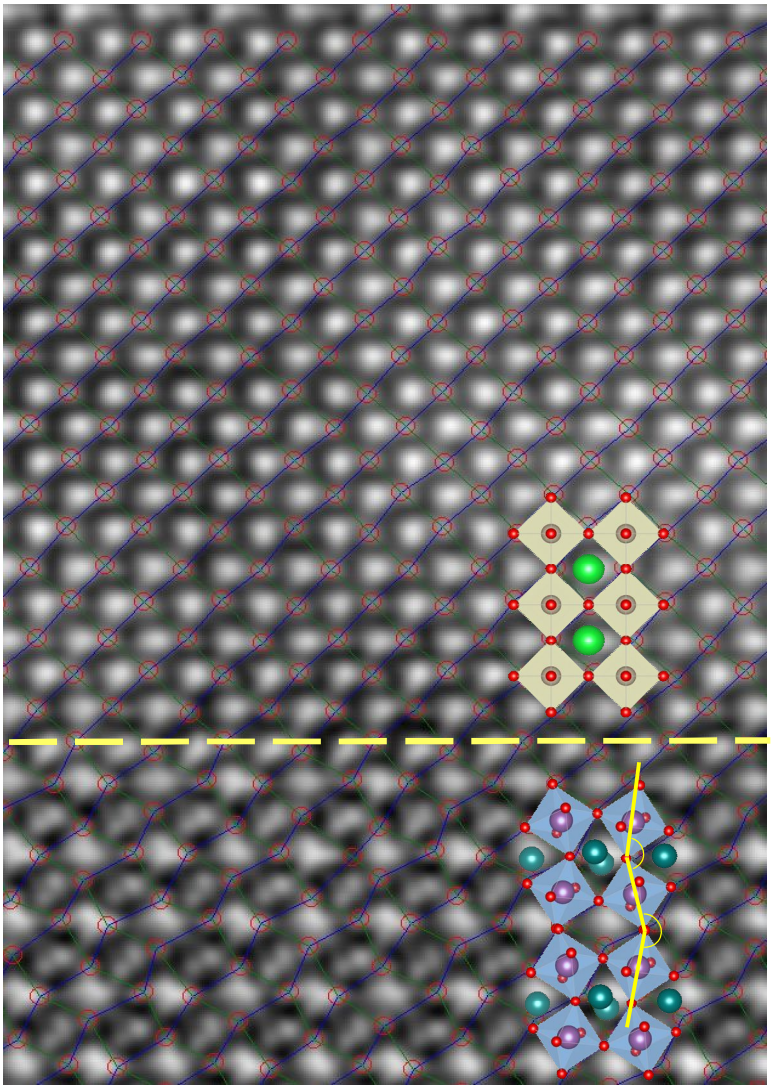

**Figure 15 High magnification HRSTEM-ABF image of interface area in 24nm SRO on GSO substrate. Superimposed illustration shows the octahedral rotation pattern of SRO and GSO respectively. Yellow dashed line is the interface.**

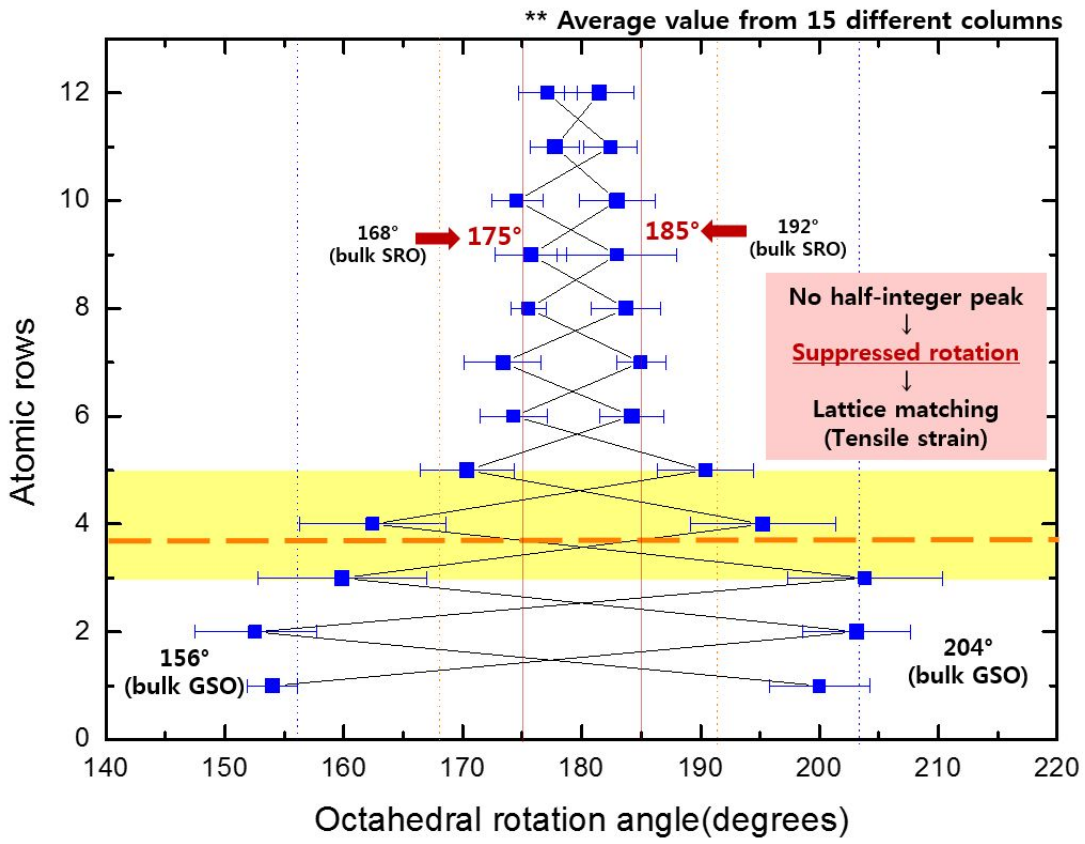


**Figure 16 Quantitative graph of octahedral rotation angle across the SRO/GSO interface obtained from ABF image (Fig 15)**

layers, the entire film region has 175° rotation angle, which is larger than that of bulk SRO, 168° . In other words, we quantitatively confirmed SRO film has much released octahedral rotation. This releasement is interpreted as the result of lattice mismatch, where tensile strain is accommodated through stretching out Ru-O-Ru bond. The gradual change near the interface including top layer of GSO substrate is ascribed to symmetry mismatch from the effect of orthorhombic GSO.

### 4.2.2 $SrTiO_3$ thin films on $SrTiO_3$

As mentioned before, on cubic STO substrates, SRO film can grow with its (001), (110) or (1-10) planes parallel to STO (001) plane. Thus, there are six possible orientations in total. However, due to pseudo-cubic characteristic of SRO, only three of them are distinguishable by means of TEM.[20] Based on **Fig 17**, it is seen that our SRO thin film has atomically flat interface with STO substrate. FFT diffraction patterns shows that this SRO film is consists of two different types of domains. **Fig 17 (b)** exhibits 1/2(001)pc peak so that we can determine that c-axis is lying in-plane and it is identified to be [1-10] zone axis. On the other hand, **Fig 17 (c)** has no half-integer peak at all, which can be regarded as diminishment or disappearance of half-inter peak due to released octahedral rotation. As octahedral rotation is more easily reduced along [001] than other axes, we assumed this belongs to [001] zone axis where the c-axis is parallel to the in-plane. Therefore, we conclude SRO films on STO are composed of two types of 90° rotational domain structures which are randomly distributed having nearly the same volume fraction (Not shown here). They are drawn in **Fig 18**. Again, the exact same results have been found in 24nm SRO on STO and we could not find any thickness dependency.

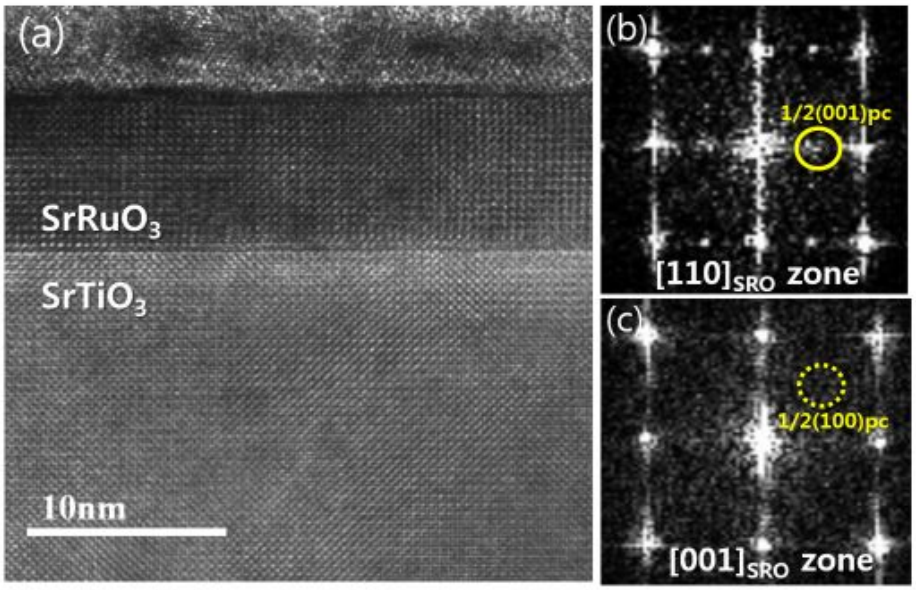


**Figure 17 HRTEM image and FFT diffraction pattern of 8nm SRO/STO (a) HRTEM image near interface, (b), (c) FFT pattern from different region in SRO thin film**

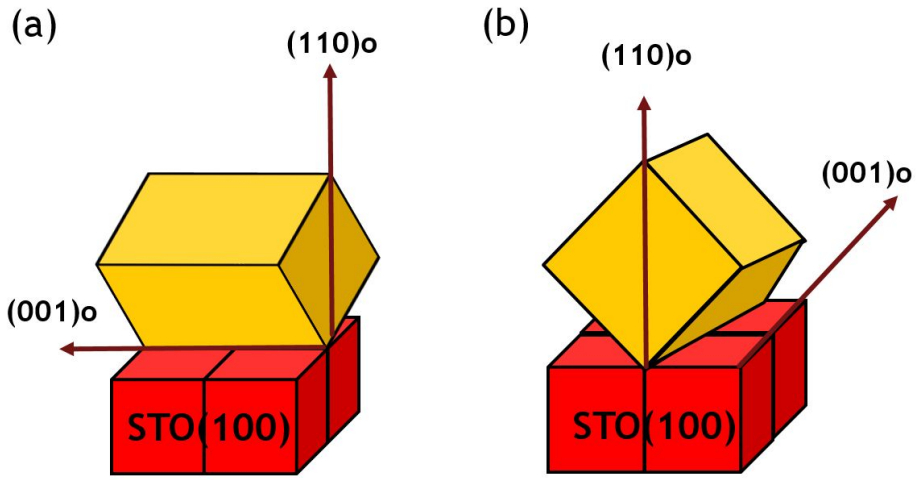


**Figure 18 Schematic image of two types of 90° rotational domain structures we found in SRO thin films**

**Fig 19** is low magnification HRSTEM-HAADF and ABF image. It is seen that SRO film is grown coherently on STO substrate. In high magnification ABF image, as shown in **Fig 20**, almost no octahedral rotation is visible. To quantitatively determine rotation angle, the same method used for SRO/GSO system was conducted again. **Fig 21** is showing the octahedral rotation angle pattern across the interface which is obtained from no half-integer region. As expected, STO substrate exhibits the same rotation angle with that of bulk STO. Surprisingly, the entire SRO film shows much released octahedral rotation angle not only around the interface region but also above two unit cell layers. The interface area can be regarded as the symmetry effect of STO cubic substrate, but the above region having much bigger rotation angle is note explainable with compressive strain effect only. These unexpected results can be the effect of symmetry mismatch but generally symmetry effect is known to be valid only interface region (2-8 unit cells) so other factors could have a comprehensive influence at the same time. Further experimental study showing strain relaxation above certain thickness which is higher than ours, 24nm, is required for clarifying this issue.

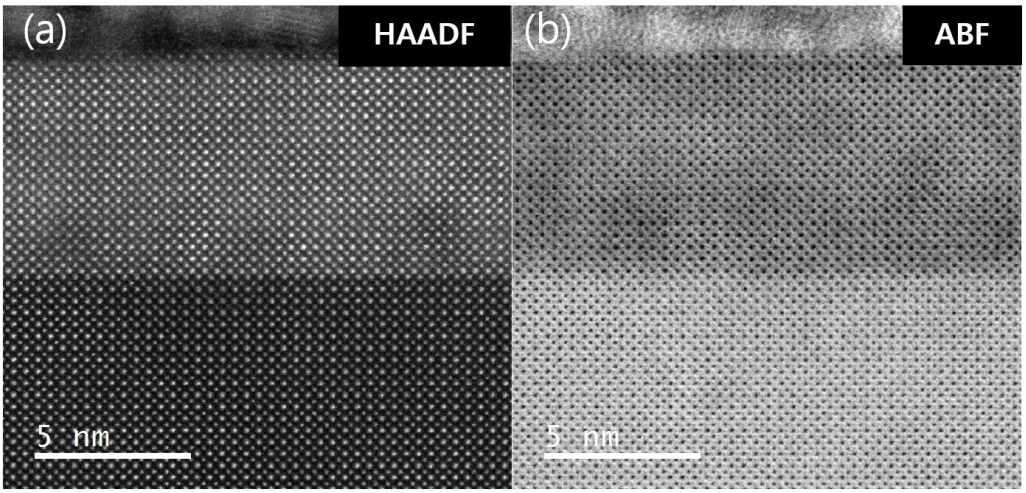


**Figure 19 Low magnification HRSTEM-HAADF, ABF images of 8nm SRO on STO substrate (a) HAADF, (b) ABF**

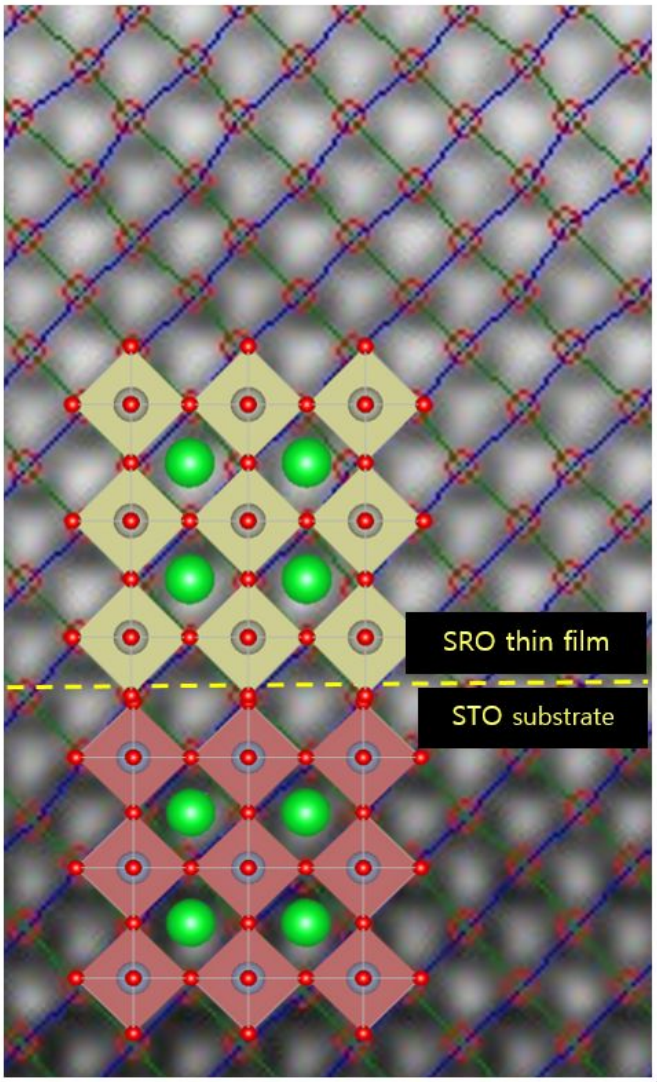


**Figure 20 High magnification HRSTEM-ABF image of 8nm SRO/STO**

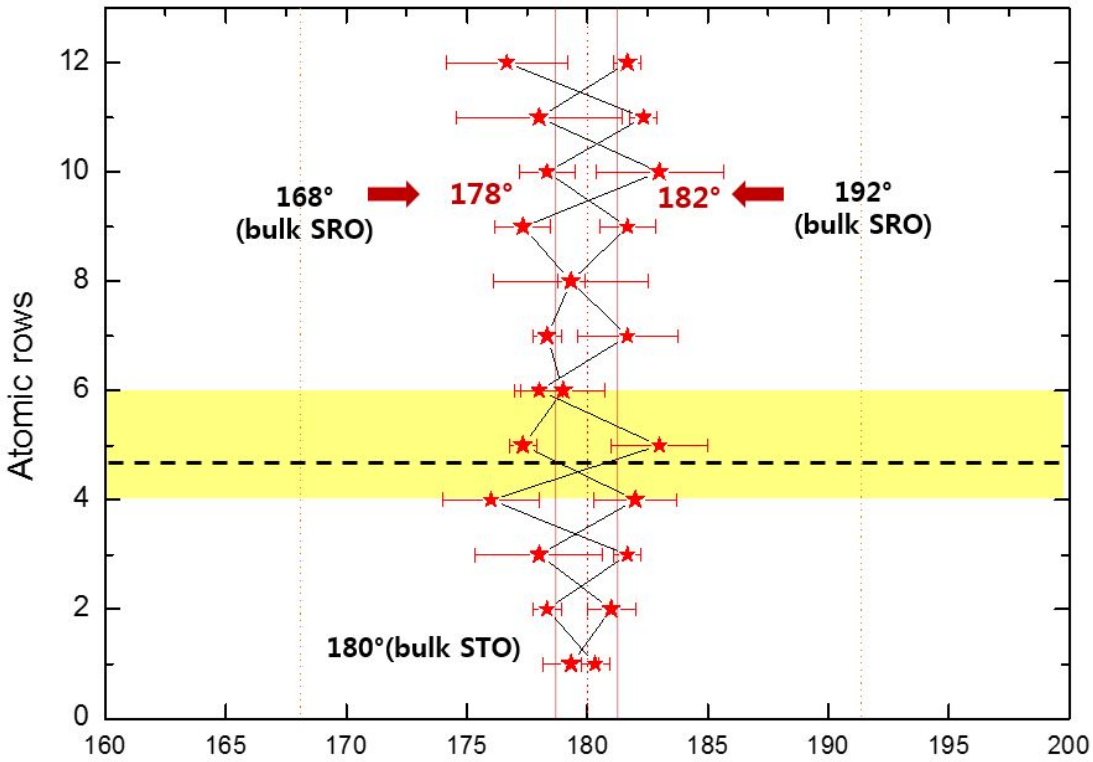


**Figure 21 Quantitative graph of octahedral rotation pattern across the SRO/STO interface obtained from ABF image (Fig 20)**

## 4.3 Physical Properties Measurement System (PPMS)

To explore the relationship between structure and electrical properties in SRO thin films, we carried out the measurement of resistivity. **Fig 22** shows the electrical resistivity of all SRO thin films plotted as a function of temperature ranging 2K-300K. It is seen that there is a sharp kink around 130K-150K. These drops in resistivity reflect the ferromagnetic transition referred to as the Curie temperature (Tc). Below Tc, SRO films show metallic behavior down to 10K. At T>Tc region, the resistivity rises almost linearly with temperature up to 300K without saturation. This behavior was previously reported by Allen[24] as a characteristic of non-Fermi liquid and utilized for defining 'bad metals' according to Emery and Kivelson[25].

Tc of all films are determined from **Fig 22** which is the curve of derivative of resistivity as a function of temperature. We cannot find distinct tendency in thickness or substrate changes at all. It can be ascribed to the uncertainty in the measurement of area/length. Also, based on TEM analysis, as we cannot find any distinct difference between SRO films on GSO and STO substrates, this results are consistent with TEM data. In addition, what we confirmed is that considering the fact that bulk SRO has the Curie temperature of 160K, all strained SRO films have reduced Tc. This is because the residual strain modified the bonding lengths and angles between ions.

[24] P.B. Allen et. al., Phys. Rev. B 48 4359 (1993)
[25] V.J.Emery and S.A. Kivelson, Phys. Rev. Lett. 74 3252 (1995)

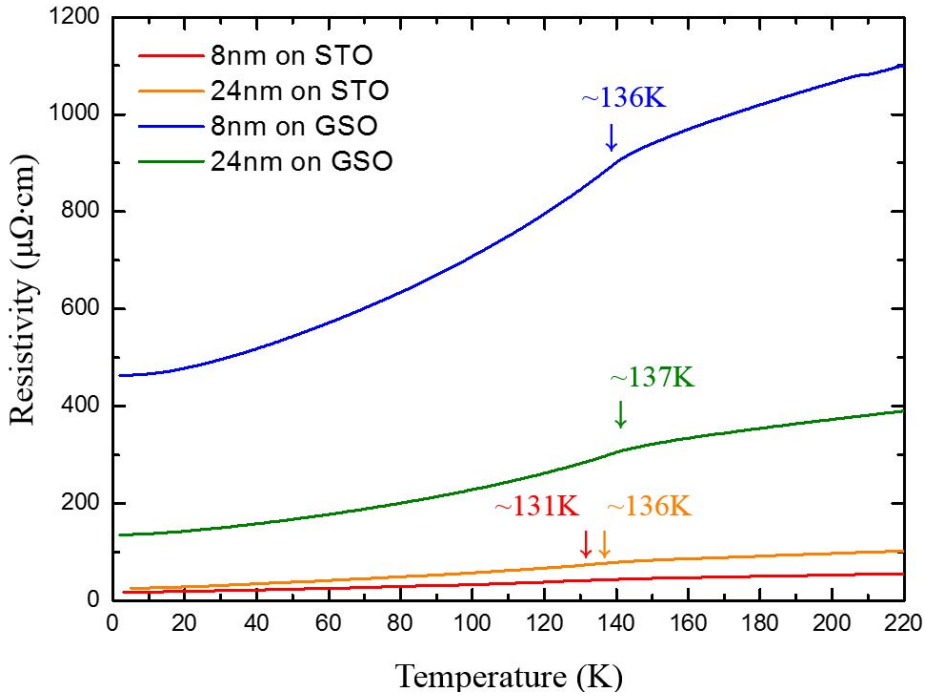


**Figure 22 Resistivity vs Temperature curve of SRO films on GSO and STO substrates**

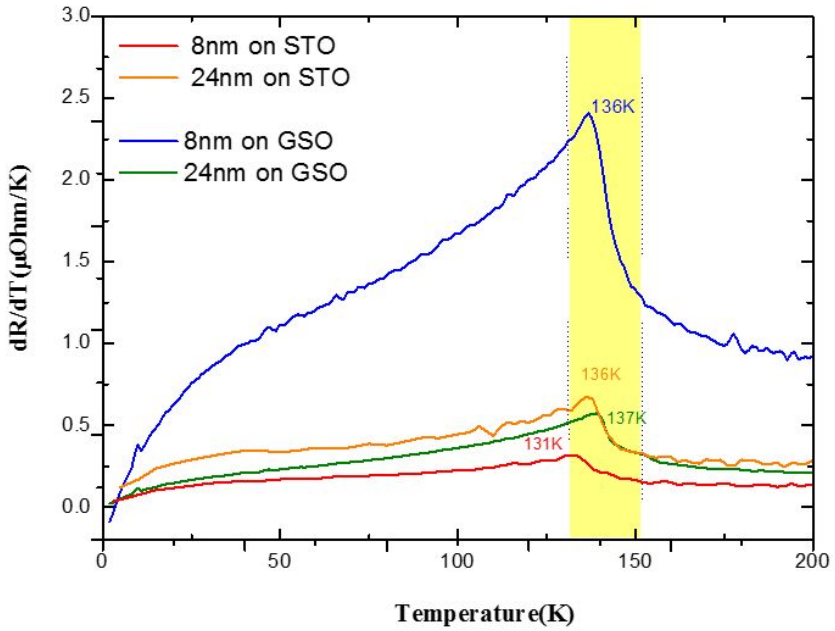


**Figure 23 The derivative of resistivity vs Temperature of SRO films on GSO and STO substrates**

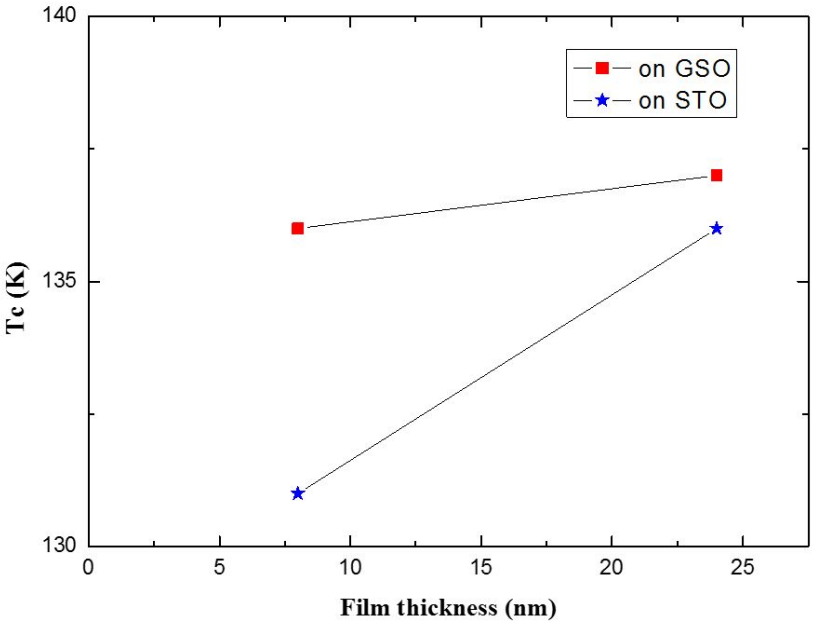


**Figure 24 Thickness dependency of Tc in SRO films on GSO and STO substrates**

# Chapter 5. Conclusion

In conclusion, we investigated strain and symmetry effects on octahedral rotations in $SrRuO_3$ thin films. We deposited SRO thin films on two different substrates, $GdScO_3$(110) and $SrTiO_3$(100) and observed atomic scale structures using high resolution STEM-ABF technique in order to compare the effect of lattice mismatch and symmetry mismatch.

On GSO substrates, we confirmed coherent epitaxial growth with (110)o orientation of SRO which is composed of two different domains, with and without half-integer peak. The absent of half-integer peak is interpreted as released octahedral rotation resulting in disappearance of cell-doubling. Based on ABF images of released rotation region, overall SRO films exhibits enlarged rotation angle ($168^\circ \rightarrow 175^\circ$) due to tensile strain from GSO substrate except for the near- interface area. Including top layer of GSO, SRO layers near interface has distortion of $RuO_6$ octahedra caused by symmetry mismatch.

On STO substrate, among three possible orientations, only two of them were observed where c-axis is parallel to in-plane. Again, coexistence of sustained and released octahedral rotation is discovered. Quantitative analysis of released region exhibits that the whole region has less-rotated octahedral pattern ($168^\circ \rightarrow 178^\circ$) resulting from the interplay of symmetry mismatch and lattice mismatch.

Physical property measurement shows all SRO films have reduced

Tc values compared to bulk SRO because of strain effect, but there was no identified dependency on substrates or thicknesses.

# References

[1] M.B. Salamon and M. Jaime, Rev. Mod. Phy. 73, 583(2001)

[2] L.W. Martin, et. al., Mater. Sci. Eng., R 68, 89 (2010)

[3] W. Lu et. al., Phys Rev B, 88, 214115 (2013)

[4] K.J.Choi et. al., Adv. Mater. 22, 759-762 (2010)

[5] W. Lu et. al., J. Appl. Phys., 113, 063901 (2013)

[6] Y.-M. Kim et. al., Adv. Mater. 25, 2497 (2013)

[7] E. Bousquet et. al., Nature, 452, 732 (2008)

[8] V. Gopalan et. al., Nat. Mater, 10, 376 (2011)

[9] R. Aso e.t al., Sci. Rep. 3, 2214 (2013)

[10] G. Koster et. al., Rev. Mod. Phys. 84, 253 (2012)

[11] L. Antognazza et. al., Appl. Phys. Lett. 63, 1005 (1993)

[12] C. W. Jones et. al., Acta. Crystallogr, 45, 365 (1989)

[13] M. W. Lufaso et. al., Acta. Crystallogr, Sect. B:Struct. Sci. 60, 10 (2004)

[14] K. J. Choi et. al., Adv. Mater. 22, 759 (2010)

[15] Cox et. al., J. Phys. C 16, 6221 (1983)

[16] Allen et. al., Phys. Rev. B 53, 4393 (1996)

[17] Singh et. al., J. Appl. Phys. 79, 4818 (1996)

[18] G. Koster et. al., Rev. of Mod. Phys. 84, 253 (2012)

[19] Kawasaki et. al., Science 266, 1540 (1994)

[20] J. C. Jiang et. al., Appl. Phys. Lett., 72, 23 (1998)

[21] G.herranz et. al., Phys. Rev. B 71, 174411 (2005)

[22] Maria J. P. et. al., Appl. Phys. Lett. 76, 3382 (2000)

[23] A.T.Zayak et. al., Phys. Rev. B., 74, 094104 (2006)

[24] P.B. Allen et. al., Phys. Rev. B 48 4359 (1993)

[25] V.J.Emery and S.A. Kivelson, Phys. Rev. Lett. 74 3252 (1995)

# 초 록

페로브스카이트 산화물은 격자-전자 간 상호작용이 크기 때문에 작은 구조 변화에도 재료의 물성이 크게 좌우된다. 따라서 기판으로 인한 변형과 같은 외부 요인에 의한 구조 변화의 메커니즘을 제대로 이해하는 것이 필수적이다. 이번 연구에서 우리는 계면에서의 $RuO_6$ 팔면체 회전과 그에 따른 물성 변화를 분석하였다. 고배율 STEM-ABF 이미징 기법을 이용하여 원자 수준에서 팔면체 뒤틀림 현상을 관찰하여 격자 불일치와 대칭 부정합에 의한 구조 변화가 어떻게 발생하는지 관찰하였다. 우리는 $SrRuO_3$ (SRO)박막을 $GdScO_3$(GSO)와 $SrTiO_3$ (STO)기판에 증착하여 각각 인장 및 압축 변형을 가하면서 결정 대칭 부정합 조건을 설정하여 두 경우를 비교하였다. 고배율 투과 전자 현미경 이미지에서 고속 푸리에 변환 이미지를 얻어 SRO 박막이 팔면체 회전이 유지된 영역과 억제된 영역, 두 가지 도메인으로 이루어져 있음을 확인하였다. 팔면체 회전이 억제된 영역에서 고배율 STEM-ABF 이미지를 얻은 결과, GSO와 STO 기판 위 모두에서 실제로 SRO 팔면체 회전 각도가 정량적으로 크게 증가함을 확인할 수 있었다. 유일한 차이점은 계면이었는데, GSO 기판에서는 기판 상단부와 SRO 박막 경계 부근 두 개의 단위체 높이까지 어느 정도 팔면체 회전을 유지한 반면, STO 기판에서는 기판 전체에서 회전이 억제되었다. 이러한 계면에서의 차이는 대칭 부정합 효과에서 기인한다. 두 경우 모두 큰 차이 없이 두 가지 도메인이 혼합된 형태였기

때문에 실제 전기적 성질 측정 결과도 비슷한 성향을 보였다. 이번 연구는 팔면체 회전이 격자 불일치와 대칭 부정합의 상호작용으로 이해할 수 있음을 알 수 있게 하였다.

**주요어:** 변형 효과, 팔면체 회전, 격자 불일치, 대칭 부정합, STEM-ABF 이미징, $SrRuO_3$ 박막

**학 번:** 2014-21478